Soil Moisture Scatter Radio Networking With Low Power

Spyridon-Nektarios Daskalakis, *Graduate Student Member, IEEE*, Stylianos D. Assimonis, Eleftherios Kampianakis, *Graduate Student Member, IEEE*, and Aggelos Bletsas, *Senior Member, IEEE*

***Abstract*— A low-cost (6 Euro per sensor), low-power (in the order of 200 μW per sensor), with high communication range (on the order of 250 m), scatter radio sensor network is presented, for soil moisture monitoring at multiple locations. The proposed network utilizes analog frequency modulation in a bistatic network architecture (i.e., the emitter and reader are not colocated), while the sensors operate simultaneously, using frequency-division multiple access. In contrast to prior art, this paper utilizes an ultralow-cost software-defined radio reader and offers custom microstrip capacitive sensing with simple calibration, as well as modulation pulses for each scatter radio sensor with 50% duty cycle; the latter is necessary for scalable network designs. The overall root mean squared error below 1% is observed, even for the range of 250 m. This is another small (but concrete) step for the adoption of scatter radio technology as a key enabling technology for scalable, large-scale, low-power, and cost environmental sensor networking.**

***Index Terms*— Scatter radio, sensor networks, soil moisture (SM).**

I. Introduction

MODERN agriculture applications necessitate cheap, effective, low-maintenance, and low-cost wireless telemetry for various environmental parameters [1], such as environmental humidity, soil moisture (SM), barometric pressure, and temperature [2]–[5]. Continuous and dense environmental monitoring is critical to optimal crop and water management techniques, and thus wireless sensor network (WSN) technologies for microclimate monitoring in extended areas are indispensable within this topic [1]. One important environmental variable that needs careful monitoring, especially in agriculture and water management applications, is percentage SM (%SM). Prior art has offered novel SM capacitive sensors integrated with discrete wireless radio module [6], [7] or discrete processing chip [8], including ink-jet fabrication designs.

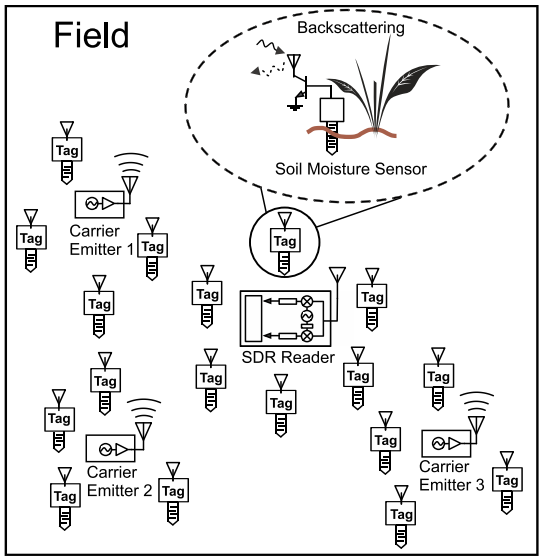

Fig. 1. Bistatic SM scatter radio WSN. There could be multiple carrier emitters and one SDR reader.

Conventional WSNs consist of a network of nodes (possibly in a mesh architecture), transferring monitored environmental data to a base station. Each node typically employs a Marconi-type radio, controlled by a microcontroller unit and the sensors. However, the large-scale deployments of conventional WSN technology are uncommon, due to power consumption, installation, and maintenance cost. Work in [9] is one rare case of large-scale, outdoor demonstration, with packaging/long-term deployment cost per wireless sensor on the order of 50 Euro.

In order to address power consumption and cost per sensor constraints, scatter radio has recently attracted interest for wireless sensing development (Fig. 1); using scatter radio, the front end of each sensor is simplified to a reflector that modulates information on the sensor's antenna-load reflection coefficient; in scatter radio, communication is performed by means of reflection, where signal conditioning, such as filtering, mixing, or amplification at the sensor/tag are typically avoided; in that way, low power consumption is needed,

Manuscript received November 2, 2015; revised February 7, 2016; accepted May 19, 2016. Date of publication June 13, 2016; date of current version July 7, 2016. This work was supported by the General Secretariat for Research & Technology through the European Union–European Social Fund and the Greek National Funds, by the National Strategic Reference Framework within the Operational Program through the ERC04-BLASE Project entitled Education & Lifelong Learning, and by the Onassis Foundation graduate studies 2015/16 scholarship.

S.-N. Daskalakis and A. Bletsas are with the School of Electronic and Computer Engineering, Technical University of Crete, Chania 73100, Greece (e-mail: sdaskalakis@isc.tuc.gr; aggelos@telecom.tuc.gr).

S. D. Assimonis was with the School of Electronic and Computer Engineering, Technical University of Crete, Chania 73100, Greece. He is now with the School of Electronics, Electrical Engineering and Computer Science, Queen's University Belfast, Belfast BT7 1NN, U.K. (e-mail: s.assimonis@qub.ac.uk).

E. Kampianakis was with the School of Electronic and Computer Engineering, Technical University of Crete, Chania 73100, Greece. He is now with the Department of Electrical and Computer Engineering, University of Washington, Seattle, WA 98195 USA (e-mail: ekampian@washington.edu).

Color versions of one or more of the figures in this paper are available online at http://ieeexplore.ieee.org.

Digital Object Identifier 10.1109/TMTT.2016.2572677

offering opportunities for batteryless operation [10], [11], e.g., each sensor can be powered using ambient radio frequency (RF) energy with appropriate rectifiers [12]–[14] or using multiple kinds of ambient energy sources, such as RF and solar energy, simultaneously [15]. Sensor designs with scatter radio typically exploit variations of sensor's antenna properties [16], based on the environmental parameter under monitoring, such as the (mechanical) shape [17] or the dielectric constant [18]; chipless designs typically include appropriately designed antenna loads with delay lines (see [19] and references therein); another way to construct scatter radio signal reflectors is by using a switch (SW), connecting sensor's antenna to different loads. Elevating the above principles from sensing to networking of several, simultaneously operating, scatter radio sensors is not trivial and emerges as a challenging topic of research.

Reference [20] offered frequency-modulated scatter radio signals with SM information and duty-cycled operation that reduced the operating bandwidth, while experimental results were reported for only two sensors and commodity software-defined radio (SDR) (with cost on the order of 1000 Euro). The tag-to-reader communication range was on the order of 100 m. In this paper, 50% duty cycle of frequency-modulated SM is achieved with a new circuit, which also reduces the overall power consumption; 50% duty cycle is crucial to getting rid of even-order harmonics and thus, enhancing the available bandwidth for multiple scatter radio sensors' simultaneous access [21]. Moreover, this paper offers a different, more accurate sensor calibration method. Moreover, this work offers experimental results for multiple sensors, ranges in the order of 250 m with ultra low-cost, portable SDR (that costs 7 Euro), while scalability issues are further examined.

A. Scatter Radio Principles

Scatter radio communication, known from 1948 [22], is currently exploited in the RF identification (RFID) industry. Communication is implemented with an antenna, a control circuit, and an RF SW between them. The SW alternatively terminates the tag/sensor antenna between (usually two) loads Z_1 and Z_2 (Fig. 2). The control circuit is responsible for the modulation operation. Tag/sensor antenna S_{11} parameter (i.e., reflection coefficient Γ), associated with each antenna terminating load, is modified when the antenna load is changed. The different termination loads offer different reflection coefficients, (Γ_1 and Γ_2) according to the following [23]–[27]:

$$\Gamma_i = \frac{Z_i - Z_{\mathrm{a}}^*}{Z_i + Z_{\mathrm{a}}} \tag{1}$$

with $i = 1, 2$ and Z_{a} denoting the antenna impedance.

Therefore, amplitude and phase of the carrier signal—induced at the sensor antenna—are modulated and the signal is reflected (scattered) back toward a receiver. As a result, when a continuous wave with frequency F_{c} is incident on the sensor antenna, which is alternatively terminated between two loads at a rate F_{sw}, two new subcarrier frequencies appear in the spectrum (Fig. 2); their frequency values are given by [28]

$$F_{\mathrm{sub},1} = F_{\mathrm{c}} + F_{\mathrm{sw}} \tag{2}$$

$$F_{\mathrm{sub},2} = F_{\mathrm{c}} - F_{\mathrm{sw}}. \tag{3}$$

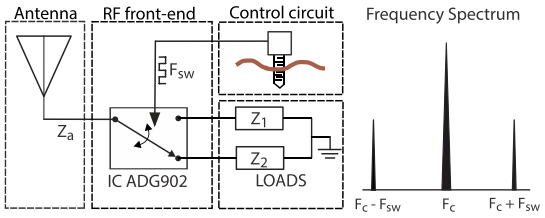

Fig. 2. Scatter radio principles. The low power RF SW ADG902 alternates the termination loads Z_1 and Z_2 of the antenna (corresponding to reflection coefficients Γ_1, Γ_2, respectively) with frequency F_{sw}. When the illuminating carrier frequency is F_{c}, two new subcarrier frequencies $F_{\mathrm{c}} \pm F_{\mathrm{sw}}$ appear in the spectrum. Difference $|\Gamma_1 - \Gamma_2|$ should be maximized; however, practical constraints (e.g., parasitics) restrict such maximization.

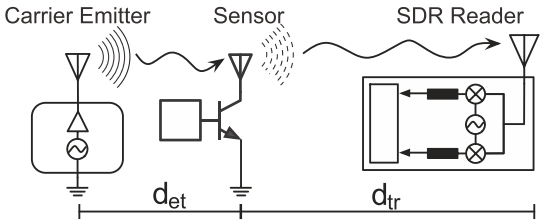

Fig. 3. Bistatic topology of a scatter radio link; emitter produces the carrier signal, which is modulated by sensor nodes and finally, the reflected signal is received by an SDR reader. d_{et} and d_{tr} denote emitter-to-tag and tag-to-reader distance, respectively. Notice that in this paper, one emitter illuminates multiple tags, simultaneously.

While scatter-radio principles have been restricted to the communication ranges of up to a few meters [29]–[31], a novel scatter radio sensor network (WSN) for relative humidity measurements was presented in [32]. The WSN consisted of the low-power and low-cost analog designs of wireless transmitters (sensor nodes/tags) with scatter radio and extended communication ranges. Each tag employed bistatic semipassive scatter radio principles [33]. In order to address the small communication range problem, the WSN utilized the bistatic topology (where the carrier emitter was placed in a different location from the reader) and semipassive (i.e., battery-assisted) tags. The utilization of the bistatic topology is shown in Fig. 3. Using the above concepts, it was shown possible to implement large-scale networks, comprising low-cost sensor/tags, a few emitters operating at the European RFID band (865–868 MHz) [34] and a single SDR receiver, detecting the backscattered signals.

This paper describes the development of a bistatic scatter radio WSN that measures %SM with analog, frequency modulation (FM) principles, and ranges on the order of 250 m. In sharp contrast to prior art, this paper offers: 1) custom capacitive sensing; 2) SM sensing and networking of multiple sensors (with corroborating experimental results); 3) reception with ultralow-cost SDR that costs only a few Euros; and 4) special modulation design that offers scatter radio modulation signals with 50% duty cycle; the latter will be shown to be important for signal-to-noise ratio improvements at the SDR receiver, as well as for network scalability purposes.

Section II offers the design and implementation of the scatter radio sensor circuit, multiple access capability, and power consumption tradeoff. Section III offers the

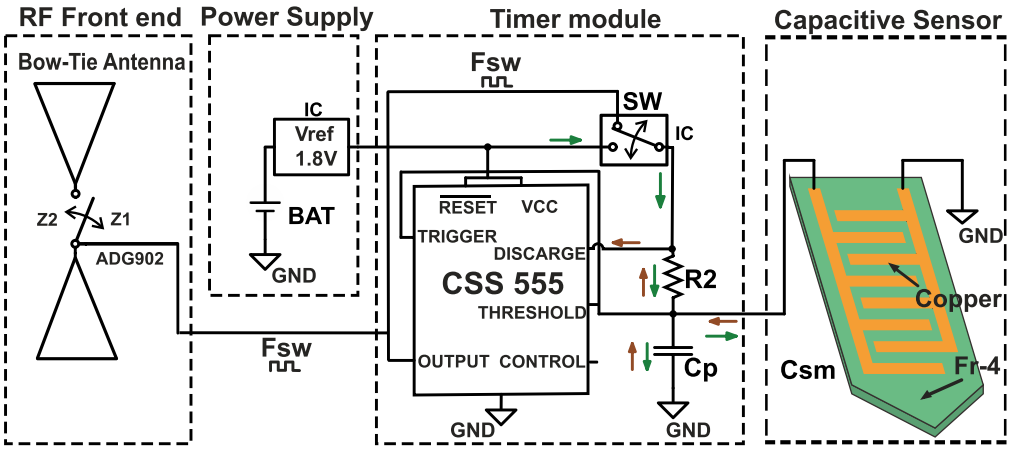

Fig. 4. Analog backscatter sensor node schematic. Each node consists of the capacitive SM sensor to be inserted in the soil, the timer module that converts the variable capacitance to frequency (C2F), and the scatter radio front end. The variable frequency signal controls the antenna RF SW. The node is supplied by a voltage reference circuit.

SDR receiver design, based on a 8-b ultralow-cost SDR, Section IV describes the simple calibration procedure and Section V offers the experimental results, including a relevant network demonstration and bistatic range measurements. Finally, the conclusion is drawn in Section VI.

II. Sensors Design and Implementation

The design target of the tags is to produce the voltage pulses of fundamental frequency that depends on the %SM value and control the rate with which the antenna termination loads are alternated. For this purpose, the circuit diagram of Fig. 4 was designed, consisting of a custom capacitive SM sensor, the C2F converter, the power supply circuit, and the scatter radio front end.

A. Sensor and C2F Converter

A single astable multivibrator circuit with 555 timer functioned as the C2F converter. The timer was the ultralow power monolithic CSS555 [35] with minimum current consumption of 5 μA at 1.2 V. The timer was connected to a resistor–capacitor network of R_2 and C_p and to the custom, microstrip capacitive sensor $C_{\rm sm}$ (Fig. 4). The capacitive sensor consisted of two isolated conductive plates, separated by a narrow gap, on low-cost FR-4 substrate with the thickness 1.5 mm and dielectric constant $\epsilon_{\rm r} = 4.6$; waterproofness was facilitated using the green solder mask as insulation. The followed capacitance sensor design is equivalent to a number of coplanar plate capacitors, inserted in parallel into the soil, which alters the dielectric constant; if the soil is moist (high %SM), the capacitor will contain more water, resulting in higher capacitance (i.e., high $C_{\rm sm}$), while the dry soil offers lower capacitance.

The fundamental frequency $F_{\rm sw}$ of the pulse depends on the resistor and the capacitor, connected to the TRIGGER and THRESHOLD pins of the 555 timer. As shown in Fig. 4 (arrows), the parallel capacitors (C_p and $C_{\rm sm}$) are periodically charged and discharged through R_2 and an electronic, single-pole single-throw (SPST) SW. The SW is open when timer output is in logic low, so there is no leakage current through the SW loop and has been placed in order to reduce consumption while attaining pulses with duty cycle of 50%; the latter is a fundamental difference compared with other C2F converters in the literature [32]. The timer output square wave pulse is offered with fundamental frequency given by

$$F_{\rm sw} = \frac{1}{2\ln(2)R_2(C_p + C_{\rm sm})}. \tag{4}$$

According to [36], the power of the fundamental subcarrier frequency of the scattered signal is given by

$$P(a) = \left[\frac{A\sqrt{2}}{\pi}\sin(\pi D)\right]^2 \tag{5}$$

where A is the peak-to-peak amplitude of the pulse signal and D is the duty cycle; thus, the backscattered signal power will be increased when D approaches the value of 50%. Using a single analog SW (SW in Fig. 4) and only one resistor (R_2) in the typical astable multivibrator circuit, the duty cycle of the produced pulse is calculated as follows:

$$D = \frac{R_2}{2R_2} = 50\%. \tag{6}$$

According to its Fourier series analysis, a 50% duty-cycle square pulse consists of odd-order harmonics of the fundamental frequency, i.e., even-order harmonics are not present. Therefore, square waves without 50% duty cycle occupy additional bandwidth, limiting the capacity of the designed network in a specific frequency band.

B. Scatter Radio Antenna/Front End

The scatter radio front end of each tag [Fig. 5 (bottom-right)] consists of a microstrip bow-tie antenna on low-cost FR-4 substrate with an embedded RF SW; the latter is the analog devices ADG902 [37], setup as SPST SW. The ADG902 was chosen due to its low insertion loss (0.8 dB at 1 GHz) and high isolation (43 dB at 1 GHz). The front-end design was tuned around 868 MHz, according to the maximization principles in [27].

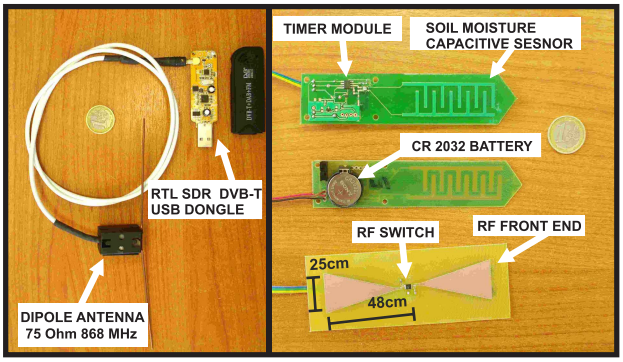

Fig. 5. Fabricated sensor node/tag (right). The green solder mask has been used as sensor insulation. Capacitive sensor and antenna/scatter radio front end are fabricated on low-cost FR-4 substrate. The Realtek (RTL) SDR reader (left) is ultralow cost on the order of 7 Euro.

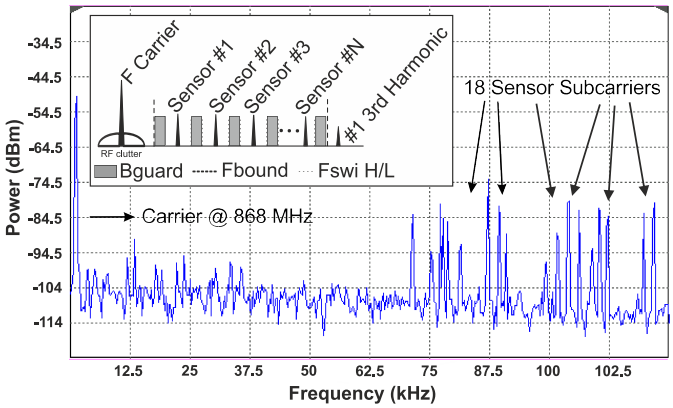

Fig. 6. Inlay figure with concept and FDMA of simultaneously operating multiple tags; each tag operates in a different frequency band, while guard bands avoid adjacent-channel interference. Measured sensor network spectrum for sensors #1–18.

A bow-tie antenna for each sensor design was adopted, due to its omnidirectional attributes (at the vertical to its axe level) and the ease of fabrication, with nominal gain of $G = 1.8$ dBi. Fig. 5 offers dimensions. Such an antenna is appropriate for the bistatic scatter radio topology, while a different printed antenna with higher gain could increase the ranging distance in the bistatic topology; however, appropriate alignment during installation could be needed in that case.

C. Multiple Access

The simultaneous, collision-free operation of multiple, receiverless sensors is facilitated with frequency-division multiple access (FDMA) principles [21], [28], [32]; every tag is assigned a distinct frequency band (bandwidth), within which the switching rate (i.e., subcarrier frequency) of each tag's antenna load can vary. Fig. 6 shows the concept with both conceptual and experimental data.

Let $F^L_{\mathrm{sw,i}}$ and $F^H_{\mathrm{sw,i}}$ denote the subcarrier frequency output of the ith tag for lowest and highest frequency, produced by the C2F converter when the %SM is 100 and 0, respectively. The required bandwidth B_i depends on the above two frequencies and is calculated as

$$B_i = F^H_{\mathrm{sw},i} - F^L_{\mathrm{sw},i}. \tag{7}$$

Assuming that C_L and C_H are the C_{sm} sensor capacitance for 0% SM and 100% SM, respectively, the $C_{\mathrm{p,i}}$ and $R_{2,\mathrm{i}}$ components of the ith tag are calculated according to (4) and (7) as

$$C_{\mathrm{p,i}} = \frac{-B_i\ C_L + F^L_{\mathrm{sw,i}}\ (C_H - C_L)}{B_i} \tag{8}$$

$$R_{2,\mathrm{i}} = \frac{B_{\mathrm{i}}}{2\ln(2)\ F^L_{\mathrm{sw,i}}\ (C_H - C_L)\ \left(F^L_{\mathrm{sw,i}} + B_i\right)}. \tag{9}$$

It is noted that the outdoor environment temperature variations affect each sensor's circuit operation. For example, the CSS555 timer exhibits a temperature drift of 40 ppm/°C and thus, for a tag/sensor with nominal subcarrier frequency at 105 kHz, an extreme change of 30 °C in temperature offers a frequency drift of $(40 \times 30 \times 105\,000)/10^6 = 126$ Hz. For the bandwidth of 1.5 kHz per sensor, the aforementioned frequency shift amounts to $126/1500 = 8.4\%$ of each sensors bandwidth and a SM error in the same order. For ten times higher bandwidth per sensor, that drift would amount to only 0.84% of error, with however reduced number of sensors in the available spectrum band. Thus, there is clearly a flexible tradeoff between scalability (in the number of simultaneously operating sensors) and measurement accuracy.

For example, assuming operating (subcarrier) sensors' frequencies in 100–299 kHz, and the guard band of 1 kHz (to avoid adjacent-channel interference between sensors) and 1.5 kHz bandwidth/sensor, the capacity of the network results to 79 sensors. An upper limit of 299 kHz is selected in order to avoid the odd-order harmonic of the lower limit subcarrier frequency of 100 kHz. Future work will install low-cost envelope detector receivers in each sensor, so that a subset of the sensors operate simultaneously and thus, the same number M of the subcarrier frequencies is shared by a larger number N of sensors, where $N \gg M$ (resembling GSM network architecture, where the same frequency channel is used by eight users in time division multiple access mode).

D. Power Consumption and Tradeoff

The power supply circuit of each sensor is a crucial part, since its lifetime depends on it. For this purpose, a voltage reference integrated circuit (IC) and a coin battery were utilized. The power source was a 300 mAh, 3 V lithium-ion battery (type CR2032), connected with the C2F converter through the voltage reference component (Texas Instruments REF3318 [38]). The voltage reference consumed 5 μA only and supplied with stable voltage (V_{cc}) the whole circuit.

The total power dissipation of each sensor is calculated below

$$P_{\mathrm{sensor}} = P_{\mathrm{charge}} + P_{\mathrm{quiescent}} \tag{10}$$

with P_{charge}, the average power required for charging the capacitors and $P_{\mathrm{quiescent}}$, the quiescent power dissipated by the timer and the voltage reference IC. The components that were utilized in the sensor design consumed quiescent power of $P_{\mathrm{quiescent}} = 17.87\ \mu$W. Moreover, average charging power was calculated according to [32] as

$$P_{\mathrm{charge}} = \frac{V^2_{\mathrm{cc}}}{6R_2\ln(2)}. \tag{11}$$

TABLE I
POWER CONSUMPTION EXAMPLE FOR TWO SENSOR NODES

Sensor #	V_{cc} (V)	R_2 (kΩ)	F_{sw} (kHz)	P_{tot} (μW)	Life (months)
1	1.8	3.6	70	267.7	5.2
2	1.8	0.793	150	1152	0.44

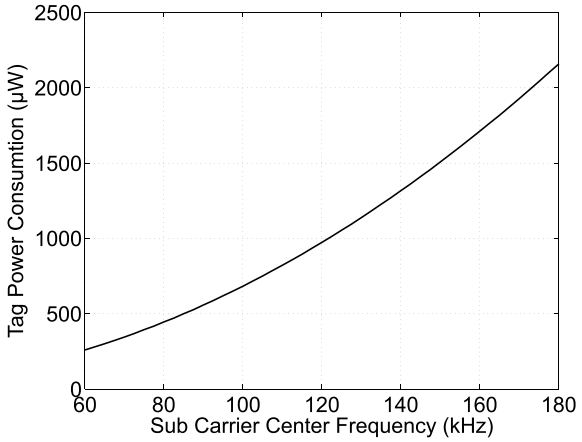

Fig. 7. Total power consumption versus sensor subcarrier frequency.

It can be seen that average power during charging P_{charge} depends on the fundamental (subcarrier) frequency, through resistor R_2. The consumption and lifetime example of two sensors is offered in Table I, including the corresponding resistor values, center frequency value, and V_{cc}. The lifetime is the duration of continuous (nonduty-cycled) operation with the utilization of the above battery. It is obvious that the lifetime of sensor #2 is too short due to the increased subcarrier center frequency. Fig. 7 shows the simulated power consumption of sensors as a function of subcarrier frequency. It is observed that when the center frequency of tags is increased from 60 to 180 kHz, the power consumption is also (nonlinearly) increased, with maximum value on the order of a milliwatt; such relatively small power can be accommodated from various ambient solar, kinetic [39], or even thermoelectric [40] sources.

Scatter radio communication also depends on the RF clutter, i.e., the increased noise power spectral density around the carrier frequency. RF clutter is created due to reflections from the surrounding environment, as well as emitter's inherent phase jitter and nonlinearities. Therefore, it is desirable for tags to operate as far as possible from the emitter's carrier frequency (i.e., as high as possible F_{sw}) in order to avoid increased noise power and hence, reduced signal-to-noise ratio. However, increased subcarrier frequency also increases power consumption and, thus, reduces sensor's lifetime.

III. ULTRALOW-COST WSN RECEIVER

One of the most important components of the scatter radio WSN is the receiver of the backscattered signals. The receiver is responsible for the fundamental frequency estimation of the incoming scattered subcarrier signals. In this paper, the ultralow-cost RTL SDR was employed, which uses a DVB-T TV tuner dongle based on the RTL2832U chip [Fig. 5 (left)]. It consists of an RF front end and the Rafael Micro R820T tuner with frequency band range of 24–1766 MHz. The small cost on the order of a few Euros comes at the price of low dynamic range, since RTL offers only 8-b resolution analog-to-digital converted samples, pushed to a host computer through USB. Processing of the in-phase and quadrature signals is done solely in software at the host computer. A dipole 75-Ω antenna was also designed to operate around 868 MHz. After a miniature coax connector for the antenna, there is a low noise amplifier with noise figure of about 3.5 dB.

The fundamental subcarrier frequency $\hat{F}_i$ of the ith sensor was estimated using the periodogram technique, which in turn is grounded on maximum likelihood principles. The estimated subcarrier was given according to

$$\hat{F}_i = \underset{F\in\left[F^L_{\text{sw,i}},F^H_{\text{sw,i}}\right]}{\arg\max} |X(F)|^2 \tag{12}$$

where $X(F)$ is the Fourier transform of the baseband down-converted and carrier frequency offset (CFO)-compensated signal. CFO estimation and compensation was based on standard periodogram techniques [41]. $F^L_{\text{sw,i}}$ and $F^H_{\text{sw,i}}$ mark the *a priori* known lowest and highest possible frequency outputs of the ith tag. Thus, the frequency component with the maximum power at each spectrum band is estimated as the corresponding sensor's output frequency.

IV. CALIBRATION

Deviations from nominal values of each tag's components (e.g., the tolerance of capacitors, resistor, or timer), as well as temperature dependence, require compensation, i.e., sensor calibration; the tags of this paper were calibrated using polynomial surface fitting, utilizing both %SM and temperature parameter as input variables, as described below.

A soil sample was taken from the field, dried, and filled a 1000- cc container. Specific mass of water (in gram) was poured into the container and %SM by volume was calculated, according to the following:

$$\text{Soil moisture}(\%)\text{ by volume} = \frac{\text{Volume of water}}{\text{Volume of soil}} \times 100 \tag{13}$$

with

$$\text{Volume of water} = \frac{\text{Mass of water}}{\text{Density of water}} \tag{14}$$

with (well-known) density of water equal to 1 g/cc.

Using the sensor design and the WSN reader described above, the samples of the subcarrier frequency were collected, for fixed temperature and variable %SM (or vice versa). Working with 226 sets of measurements (subcarrier frequency, temperature, and SM), minimum mean square error (MSE) cubic polynomial fitting was applied between subcarrier frequency, %SM and temperature. The outcome polynomial is given in Table II with corresponding fitting root mean squared error (RMSE). The surface (3-D) transfer function is shown in Fig. 8 and a special case for fixed temperature 18.4°C, (2-D) transfer function is shown in Fig. 9.

Fig. 9 shows an interesting saturation effect (at the output frequency) when the SM by volume reaches 48%. That is

TABLE II
CALIBRATION FUNCTION AND FITTING ERROR

Model	Fitted function	RMSE
3D	$f(x,y) = 105.5 + 0.232x + 0.0121y - 0.0074x^2$ $+0.0020xy - 0.0036y^2 + 7.531 * 10^{-5}x^3$ $-2.94 * 10^{-5}x^2y + 2.08 * 10^{-6}xy^2 + 3.65 * 10^{-5}y^3$	0.23 (kHz)

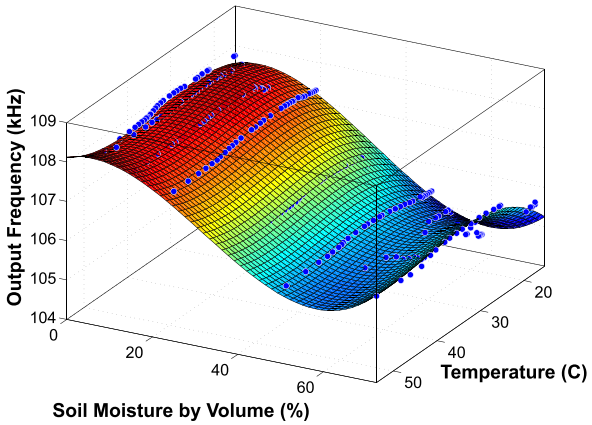

Fig. 8. Measured SM (%) characteristic and polynomially fitted function versus frequency and temperature for sensor #8. The data measurements were 226 sets of SM, temperature, and output frequency samples.

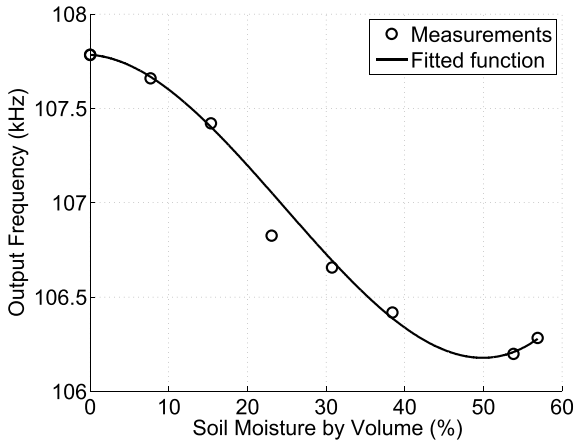

Fig. 9. Measured SM (%) characteristic and fitted function versus frequency for sensor #8 for fixed environmental temperature (18.4°C).

due to the hydraulic properties of all soil textures. Specifically, total pore space expressed on a volumetric basis, ranges from 40% in sandy soil to 48% in clay soil. When a soil is completely saturated, all the pores are filled with water. Thus, porosity is also the water content at saturation, expressed as the volume of water per volume of soil. [42, Ch. 6, p. 167]. Thus, the observed saturation above 48% of the sensor is clearly coherent with the physical phenomenon of water content in various soil textures and thus, an indirect indication that the sensor is working properly.

Measured %SM results using the above procedure of (13) and (14) were compared with the sensor's output; for the data of Fig. 9 (fixed temperature), theRMSE of 0.15% SM, and the mean absolute error of 0.13% SM were found.

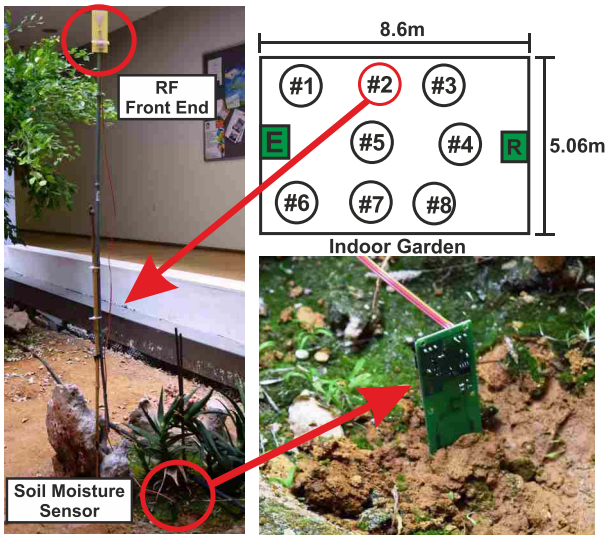

Fig. 10. Bistatic SM sensor network demonstration; capacitive SM sensor is installed into the ground, while scatter radio antenna is well above ground and being illuminated by the carrier emitter (E), while backscattered signal from various tags is received by the reader (R).

Such error will be denoted as calibration error, since it does not include the error due to scatter radio communication, studied in the following.

V. EXPERIMENTAL RESULTS

Fig. 5 (right) shows one of the fabricated sensor tags with low-cost FR-4 material and cost on the order of 6 Euro. At the installation site, each backscatter sensor node's bow-tie antenna (with its scatter radio at front end) was located well above the ground, while the fabricated capacitive sensor was inserted into the soil (Fig. 10) and the connection between those two parts was established with cables. The implemented demonstration WSN consisted of 18 scatter-radio SM sensors nodes, which could operate simultaneously, without collisions; Fig. 6 shows the obtained sensors subcarriers and the emitter carrier at 868 MHz. Each sensor was allocated a unique 0.5–1.5-kHz frequency band (bandwidth) and there was a guard band of 1 kHz between neighboring-in-frequency tags to alleviate adjacent-channel interference. Fig. 6 shows the subcarriers corresponding to 0% SM.

For demonstration purposes, a subset of the network was deployed in the indoor garden of the Technical University of Crete. The bistatic topology scatter radio WSN with eight sensor nodes is shown in Fig. 10. Carrier emitter (E) and RTL-SDR reader (R) were located at either sides of the field with the sensors in between. Capacitive sensors were inserted into the soil near the root of each plant, while the scatter radio front-ends were placed 1.5 m above the ground, using canes.

Sampled data time series collected from ∼7 h of continuous monitoring are shown in Fig. 11. It can be easily observed that after the watering instances, the output frequency of the sensors changed instantly, while it settled after a limited amount of time.

In order to achieve both the communication performance characterization and sensing accuracy of the proposed WSN,

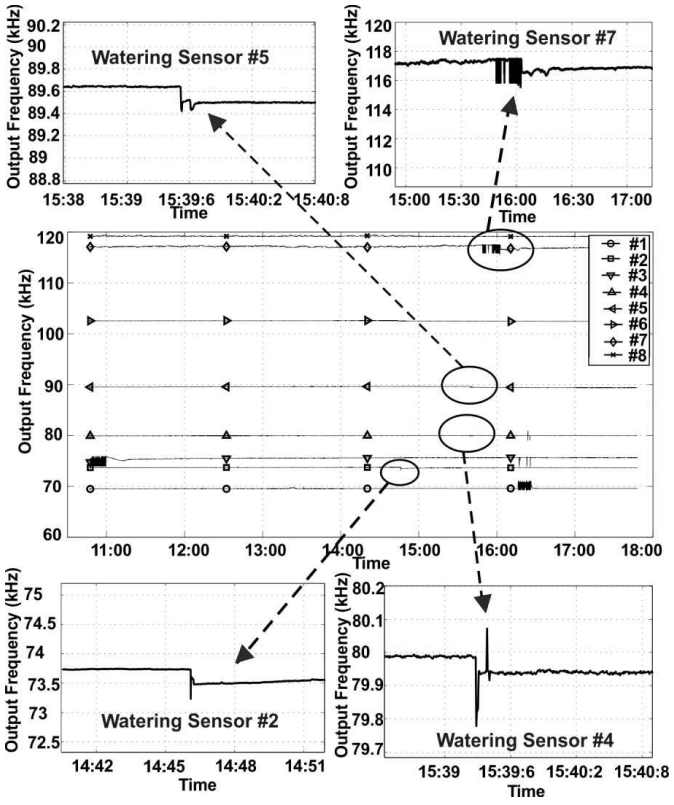

Fig. 11. Simultaneous and continuous SM sensing from eight tags, as a function of time, using the proposed scatter radio sensor network.

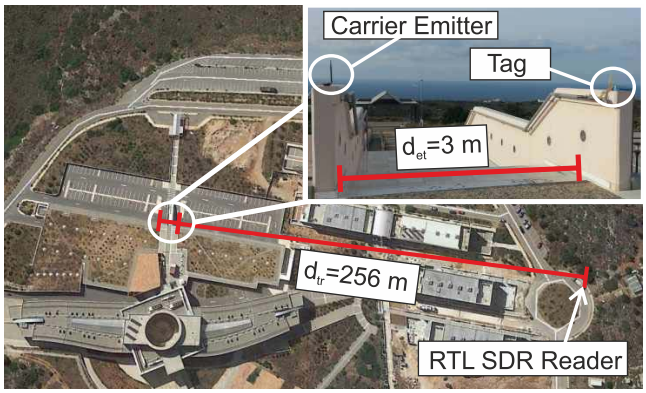

Fig. 12. Testing outdoors the communication range of the specific bistatic analog backscatter architecture.

maximum communication range and end-to-end sensing accuracy were experimentally measured. Specifically, a complete bistatic topology link was utilized outdoors (Fig. 12).

Carrier emitter, SDR receiver, and sensor/tag (with subcarrier center frequency at 109 kHz) were installed at 1.3 m height. The temperature of 18 °C was measured, SM was fixed at 0% SM (corresponding to 109 kHz subcarrier frequency for the specific sensor), sampling rate was set to 1 MHz, and the duration of 100 ms was exploited per sensor measurement. Communication performance was tested for various installation topologies and the corresponding results, in terms of estimating the transmitted subcarrier frequency, are presented in Table III, as a function of emitter-to-tag distance (d_{et}), tag-to-reader distance (d_{tr}), and RMSE in Hz, after 1000 measurements, for each case (row) of Table III. Reference subcarrier value was measured with carrier emitter and SDR receiver in closed proximity with the sensor (and all the rest of the parameters are the same), using the average value out of 1000 sensor measurements.

TABLE III
COMMUNICATION ACCURACY

#	d_{et} (m)	d_{tr} (m)	RMSE (Hz)	RMSE (%)
1	3	48.3	12.91	0.011
2	3	69	17.00	0.015
3	3	146	26.89	0.024
4	3	205	31.39	0.028
5	3	256	35.28	0.032
6	8.4	60.8	21.41	0.019
7	8.4	138	32.63	0.029
8	21.4	126	9.70	0.008

Sensor-receiver ranges on the order of 256 m are possible, with a limited RMSE error on the order of 0.1%, due to wireless communication. Such small communication error suggests that communication ranges could be further increased and scatter radio communication range is not an issue. A similar finding, based on proper designs for scatter radio reception, has also been recently reported in [43]–[45]. Therefore, the overall sensor error is upper bounded by the sum of the RMSE calibration and communication errors under mild assumptions (e.g., independence of noise in sensor and noise in receiver, unbiased errors, and so on), which for the values of Table III and the results of Section IV offer overall RMSE below 1% SM. Finally, it is noted that for all experimental results, emitter transmission power was 13 dBm at 868 MHz.

VI. CONCLUSION

This paper described in detail the development of a scatter radio network of low-power and low-cost sensors of SM. Communication ranges on the order of 250 m were experimentally demonstrated, with overall RMSE, <1%. Scaling issues were also discussed. The low power consumption of each scatter radio sensor, in the order of 200 μW, enables powering from ambient energy sources (including RF and thermoelectric), left for future work.

ACKNOWLEDGMENT

The authors would like to thank all members of the Telecom Fab Laboratory, School of Electronic and Computer Engineering, Technical University of Crete, and especially G. Vougioukas and K. Tzedaki for their help in various steps throughout this work.

REFERENCES

[1] G. Vellidis, V. Garrick, S. Pocknee, C. Perry, C. Kvien, and M. Tucker, "How wireless will change agriculture," *Precis. Agricult.*, vol. 7, pp. 57–67, Jun. 2007.

[2] M. Haefke, S. C. Mukhopadhyay, and H. Ewald, "A Zigbee based smart sensing platform for monitoring environmental parameters," in *Proc. IEEE Int. Instrum. Meas. Technol. Conf. (I2MTC)*, Binjiang, China, May 2011, pp. 1–8.

[3] G. R. Mendez, M. A. M. Yunus, and S. C. Mukhopadhyay, "A WiFi based smart wireless sensor network for monitoring an agricultural environment," in *Proc. IEEE Int. Instrum. Meas. Technol. Conf. (I2MTC)*, Graz, Austria, May 2012, pp. 2640–2645.

[4] D. Antolín, A. Bayo, N. Medrano, B. Calvo, and S. Celma, "Wubinet: A flexible WSN for applications in environmental monitoring," in *Proc. IEEE Int. Conf. Instrum. Meas. Technol. (I2MTC)*, Graz, Austria, May 2012, pp. 2608–2611.

[5] V. Palazzari *et al.*, "Leaf compatible 'eco-friendly' temperature sensor clip for high density monitoring wireless networks," in *Proc. IEEE 15th Medit. Microw. Symp. (MMS)*, Lecce, Italy, Nov./Dec. 2015, pp. 1–4.

[6] Y. Kawahara, H. Lee, and M. M. Tentzeris, "SenSprout: Inkjet-printed soil moisture and leaf wetness sensor," in *Proc. ACM Conf. Ubiquitous Comput.*, Pittsburgh, PA, USA, Sep. 2012, p. 545.

[7] S. Sulaiman, A. Manut, and A. R. N. Firdaus, "Design, fabrication and testing of fringing electric field soil moisture sensor for wireless precision agriculture applications," in *Proc. IEEE Int. Conf. Inf. Multimedia Technol. (ICIMT)*, Jeju, South Korea, Dec. 2009, pp. 513–516.

[8] S. Kim, Y. Kawahara, A. Georgiadis, A. Collado, and M. M. Tentzeris, "Low-cost inkjet-printed fully passive RFID tags using metamaterial-inspired antennas for capacitive sensing applications," in *Proc. IEEE MTT-S Int. Microw. Symp. (IMS)*, Seattle, WA, USA, Jun. 2013, pp. 1–4.

[9] Y. Liu *et al.*, "Does wireless sensor network scale? A measurement study on GreenOrbs," in *Proc. IEEE INFOCOM*, Shanghai, China, Apr. 2011, pp. 873–881.

[10] S. Kim *et al.*, "No battery required: Perpetual RFID-enabled wireless sensors for cognitive intelligence applications," *IEEE Microw. Mag.*, vol. 14, no. 5, pp. 66–77, Jul. 2013.

[11] S. D. Assimonis, S.-N. Daskalakis, and A. Bletsas, "Sensitive and efficient RF harvesting supply for batteryless backscatter sensor networks," *IEEE Trans. Microw. Theory Techn.*, vol. 64, no. 4, pp. 1327–1338, Apr. 2016.

[12] J. Kimionis and M. M. Tentzeris, "RF tag front-end design for uncompromised communication and harvesting," in *Proc. IEEE RFID Technol. Appl. Conf. (RFID-TA)*, Tampere, Finland, Sep. 2014, pp. 109–114.

[13] S. D. Assimonis and A. Bletsas, "Energy harvesting with a low-cost and high efficiency rectenna for low-power input," in *Proc. IEEE Radio Wireless Symp. (RWS)*, Newport Beach, CA, USA, Jan. 2014, pp. 229–231.

[14] S. D. Assimonis, S.-N. Daskalakis, and A. Bletsas, "Efficient RF harvesting for low-power input with low-cost lossy substrate rectenna grid," in *Proc. IEEE Conf. RFID Technol. Appl. (RFID-TA)*, Tampere, Finland, Sep. 2014, pp. 1–6.

[15] K. Niotaki, F. Giuppi, A. Georgiadis, and A. Collado, "Solar/EM energy harvester for autonomous operation of a monitoring sensor platform," *Wireless Power Transf.*, vol. 1, no. 1, pp. 44–50, Mar. 2014.

[16] S. Caizzone, E. Digiampaolo, and G. Marrocco, "Investigation of suitable parameters for setup-independent RFID sensing," in *Proc. IEEE Int. EURASIP Workshop RFID Technol. (EURFID)*, Rosenheim, Germany, Oct. 2015, pp. 98–102.

[17] C. Occhiuzzi, C. Paggi, and G. Marrocco, "Passive RFID strain-sensor based on meander-line antennas," *IEEE Trans. Antennas Propag.*, vol. 59, no. 12, pp. 4836–4840, Dec. 2011.

[18] R. Nair, E. Perret, S. Tedjini, and T. Barron, "A humidity sensor for passive chipless RFID applications," in *Proc. IEEE Int. Conf. RFID-Technol. Appl. (RFID-TA)*, Nice, France, Sep. 2012, pp. 29–33.

[19] R. Nair, E. Perret, and S. Tedjini, "Chipless RFID based on group delay encoding," in *Proc. IEEE Int. Conf. RFID-Technol. Appl. (RFID-TA)*, Sitges, Spain, Sep. 2011, pp. 214–218.

[20] S. N. Daskalakis, S. D. Assimonis, E. Kampianakis, and A. Bletsas, "Soil moisture wireless sensing with analog scatter radio, low power, ultra-low cost and extended communication ranges," in *Proc. IEEE SENSORS*, Valencia, Spain, Nov. 2014, pp. 122–125.

[21] A. Bletsas, S. Siachalou, and J. N. Sahalos, "Anti-collision tags for backscatter sensor networks," in *Proc. IEEE 38th Eur. Microw. Conf. (EuMC)*, Amsterdam, The Netherlands, Oct. 2008, pp. 179–182.

[22] H. Stockman, "Communication by means of reflected power," *Proc. IRE*, vol. 36, no. 10, pp. 1196–1204, Oct. 1948.

[23] K. Kurokawa, "Power waves and the scattering matrix," *IEEE Trans. Microw. Theory Techn.*, vol. 13, no. 2, pp. 194–202, Mar. 1965.

[24] P. V. Nikitin, K. V. S. Rao, S. F. Lam, V. Pillai, R. Martinez, and H. Heinrich, "Power reflection coefficient analysis for complex impedances in RFID tag design," *IEEE Trans. Microw. Theory Techn.*, vol. 53, no. 9, pp. 2721–2725, Sep. 2005.

[25] J. D. Griffin and G. D. Durgin, "Complete link budgets for backscatter-radio and RFID systems," *IEEE Antennas Propag. Mag.*, vol. 51, no. 2, pp. 11–25, Apr. 2009.

[26] A. Bletsas, A. G. Dimitriou, and J. N. Sahalos, "Improving backscatter radio tag efficiency," *IEEE Trans. Microw. Theory Techn.*, vol. 58, no. 6, pp. 1502–1509, Jun. 2010.

[27] S. D. Assimonis, E. Kampianakis, and A. Bletsas, "Microwave analysis and experimentation for improved backscatter radio," in *Proc. IEEE 8th Eur. Conf. Antennas Propag. (EuCAP)*, The Hague, The Netherlands, Apr. 2014, pp. 3228–3229.

[28] G. Vannucci, A. Bletsas, and D. Leigh, "A software-defined radio system for backscatter sensor networks," *IEEE Trans. Wireless Commun.*, vol. 7, no. 6, pp. 2170–2179, Jun. 2008.

[29] S. Naderiparizi, A. N. Parks, Z. Kapetanovic, B. Ransford, and J. R. Smith, "WISPCam: A battery-free RFID camera," in *Proc. IEEE Int. Conf. RFID*, Apr. 2015, pp. 166–173.

[30] Y. Zhao and J. R. Smith, "A battery-free RFID-based indoor acoustic localization platform," in *Proc. IEEE Int. Conf. RFID*, Apr./May 2013, pp. 110–117.

[31] A. Dementyev and J. R. Smith, "A wearable UHF RFID-based EEG system," in *Proc. IEEE Int. Conf. RFID*, Apr./May 2013, pp. 1–7.

[32] E. Kampianakis, J. Kimionis, K. Tountas, C. Konstantopoulos, E. Koutroulis, and A. Bletsas, "Wireless environmental sensor networking with analog scatter radio and timer principles," *IEEE Sensors J.*, vol. 14, no. 10, pp. 3365–3376, Oct. 2014.

[33] J. Kimionis, A. Bletsas, and J. N. Sahalos, "Bistatic backscatter radio for tag read-range extension," in *Proc. IEEE Int. Conf. RFID-Technol. Appl. (RFID-TA)*, Nice, France, Nov. 2012, pp. 356–361.

[34] ERC Rep. 25, 2015. [Online]. Available: http://www.erodocdb.dk/docs/doc98/official/pdf/ERCRep025.pdf

[35] Custom Silicon Solutions. (2009). *CSS555 Micropower Timer, Product Manual*. [Online]. Available: http://www.customsiliconsolutions.com/downloads/Revised%20Standard%20products/CSS555_Spec.pdf

[36] S. W. Smith, *The Scientist and Engineer's Guide to Digital Signal Processing*. San Diego, CA, USA: California Tech. Publishing, 1997.

[37] Analog Devices. (2005). *ADG902 RF Switch, Product Manual*. [Online]. Available: http://www.analog.com/media/en/technical-documentation/data-sheets/ADG901_902.pdf

[38] Texas Instruments. (2014). *REF3318 Voltage Reference IC, Product Manual*. [Online]. Available: http://www.ti.com/lit/ds/symlink/ref3318.pdf

[39] Perpetuum Inc. (2010). *Free-Standing Vibration Energy Harvester*. [Online]. Available: http://www.perpetuum.com/fsh.asp

[40] Micropelt Inc. *MPG-D651 Thermogenerator, Product Manual*. [Online]. Available: http://thermalforce.de/engl/product/thermogenerator/micropelt_d751.pdf

[41] Micropelt Inc. (2002). *MPG-D651 Thermogenerator, Product Manual*. [Online]. Available: http://thermalforce.de/engl/product/thermogenerator/micropelt d751.pdf

[42] G. B. Bonan, *Ecological Climatology: Concepts and Applications*, 1st ed. Cambridge, U.K.: Cambridge Univ. Press, 2002.

[43] J. Kimionis, A. Bletsas, and J. N. Sahalos, "Increased range bistatic scatter radio," *IEEE Trans. Commun.*, vol. 62, no. 3, pp. 1091–1104, Mar. 2014.

[44] N. Fasarakis-Hilliard, P. N. Alevizos, and A. Bletsas, "Coherent detection and channel coding for bistatic scatter radio sensor networking," *IEEE Trans. Commun.*, vol. 63, no. 5, pp. 1798–1810, May 2015.

[45] P. N. Alevizos and A. Bletsas, "Noncoherent composite hypothesis testing receivers for extended range bistatic scatter radio WSNs," in *Proc. IEEE Int. Conf. Commun. (ICC)*, London, U.K., Jun. 2015, pp. 4448–4453.

Spyridon-Nektarios Daskalakis (S'13–GSM'15) was born in Heraklion, Greece, in 1991. He received the Engineering Diploma (Hons.) degree in electronic and computer engineering from the Technical University of Crete, Chania, Greece, in 2014, where he is currently pursuing the M.Sc. degree.

His current research interests include low-cost wireless sensor networks and RF energy harvesting, in particular, scatter radio networking, batteryless sensors, PCB design, low cost software defined radio, environmental sensing, and RF energy harvesting.

Dr. Daskalakis was a recipient of the Fellowship Award for his project Aristeos (olive fly detection and monitoring with wireless sensor network) from Clinton Global Initiative University, Phoenix, AZ, USA, in 2014, and the Onassis Foundation Graduate Studies 2015 and 2016 Scholarship.

Stylianos D. Assimonis received the Diploma/M.Eng. and Ph.D. degrees in electrical and computer engineering from the Aristotle University of Thessaloniki, Thessaloniki, Greece, in 2005 and 2011, respectively.

He was with the School of Electronic and Computer Engineering, Technical University of Crete, Chania, Greece, and the Radiocommunication Laboratory, School of Physics, Aristotle University of Thessaloniki, as a Post-Doctoral Researcher, from 2012 to 2015. He is currently a Senior Research Fellow with Queen's University Belfast, Belfast, U.K. His research interests span electromagnetism, RF/microwave/millimeter wave technologies, antennas, metamaterials, and wireless communications.

Dr. Assimonis was the recipient of the Postdoctoral Scholarship for Excellence from the Research Committee of Aristotle University of Thessaloniki, in 2012, and a corecipient of the Metamaterials 2013 Best Paper Award (3rd place), the 2014 IEEE RFID-TA Best Student Paper Competition Finalist, and the 2015 5th COST IC1301Workshop Best Student Paper Award (third prize).

Eleftherios Kampianakis (GSM'13) received the Engineering Diploma and M.Sc. degrees in electronic and computer engineering from the Technical University of Crete, Chania, Greece, in 2011 and 2013, respectively, and is currently pursuing the Ph.D. degree at the University of Washington, Seattle, WA, USA.

He is developing implant systems for spinal cord injury treatment with the University of Washington. As an Undergraduate Researcher, he developed "over the air" programmed WSN testbeds with low-power software defined radio transceivers. As a Graduate Researcher during his M.Sc. studies he developed low-power, low-cost, and large-scale scatter radio WSN.

Dr. Kampianakis was a recipient of a Fellowship Award for his graduate studies, the Best Diploma Thesis Award-IEEE Vehicular Technology Society and Aerospace, and Electronic Systems Society's Joint Greece Chapter Final/Diploma Thesis Competition.

Aggelos Bletsas (S'03–M'05–SM'14) received the Diploma (Hons.) degree in electrical and computer engineering from the Aristotle University of Thessaloniki (AUTh), Thessaloniki, Greece, in 1998, and the S.M. and Ph.D. degrees from the Massachusetts Institute of Technology (MIT), Cambridge, MA, USA, in 2001 and 2005, respectively.

He was with Mitsubishi Electric Research Laboratories, MIT, as a Post-Doctoral Fellow, and the Radiocommunications Laboratory, Department of Physics, AUTh, as a Visiting Scientist. He joined the School of Electronic and Computer Engineering, Technical University of Crete, Chania, Greece, in 2009, as an Assistant Professor, where he was promoted to Associate Professor in 2014. He holds two patents from the U.S. Patent and Trademark Office. His current research interests include scalable wireless communication and networking, with an emphasis on relay techniques, backscatter communications and RFID, energy harvesting, radio hardware/software implementations for wireless transceivers, and low-cost sensor networks, and single-transistor frontends and backscatter sensor networks for large-scale environmental sensing.

Prof. Bletsas was a corecipient of the IEEE Communications Society 2008 Marconi Prize Paper Award in Wireless Communications, the Best Paper Distinction at ISWCS 2009, Siena, Italy, the Second Best Student Paper Award at the IEEE RFID-TA 2011, Barcelona, Spain, the Best Paper Distinction at the IEEE Sensors Conference 2013, Baltimore, MD, USA, and the Best Student Paper Award at the IEEE ICASSP 2015, Brisbane, QLD, Australia. He was a recipient of the Technical University of Crete 2013 Research Excellence Award in 2013. Two of his undergraduate advisees were winners of the 2009–2011 and 2011–2012 Best Diploma Thesis Contest, respectively, among all Greek Universities on Advanced Wireless Systems by the IEEE VTS/AES joint Greek Chapter. He is the Principal Investigator (PI) of project BLASE: Backscatter Sensor Networks for Large-Scale Environmental Sensing, funded from the General Secretariat of Research & Technology Action "Proposals evaluated positively from the 3rd European Research Council (ERC) Call." He is the Management Committee Member and National Representative in the European Union COST Action IC1301 Wireless Power Transmission for Sustainable Electronics. He has been an Associate Editor of the IEEE WIRELESS COMMUNICATION LETTERS since its foundation, an Associate Editor of the IEEE TRANSACTIONS ON WIRELESS COMMUNICATIONS, and a Technical Program Committee Member of flagship IEEE conferences.